Table 5. *Calculated parameters versus the sample height* (h), *at a fixed radius* $R = 1$ cm, *at different values of the sample attenuation coefficient* μ *and at two values of the vanadium cell thickness* t

Results refer to the scattering angle $2\theta = 50°$. (*a*) Double-scattering parameter m (%); (*b*) γ coefficient.

(*a*) Vanadium cell; double-scattering parameter m

μ (cm^{-1})	1	3·33	5	10	
			h (cm)		
0·1	8·34	12·9	14·3	16·3	
0·3	18·3	27·1	29·7	33·8	$t = 0·05$ cm
0·5	26·4	38·1	41·6	47·6	
0·1	10·4	16·5	18·2	20·8	
0·3	20·3	30·4	33·3	37·9	$t = 0·10$ cm
0·5	28·4	41·3	45·2	51·7	

(*b*) Vanadium cell; γ coefficient

μ (cm^{-1})	1	3·33	5	10	
			h (cm)		
0·1	0·887	0·886	0·886	0·885	
0·3	0·710	0·708	0·708	0·706	$t = 0·05$ cm
0·5	0·582	0·580	0·579	0·578	
0·1	0·892	0·891	0·890	0·889	
0·3	0·722	0·720	0·719	0·717	$t = 0·10$ cm
0·5	0·600	0·597	0·596	0·594	

The present program will be made available to interested parties on request.

References

BELLISSENT-FUNEL, M. C., BUONTEMPO, U., PETRILLO, C. & RICCI, F. P. (1989). *Phys. Rev. A*, **40**, 7346-7354.
BISCHOFF, F. G., YEATER, M. L. & MOORE, W. E. (1972). *Nucl. Sci. Eng.* **48**, 266-281.
BLECH, I. A. & AVERBACH, B. L. (1965). *Phys. Rev. A*, **137**, 1113-1116.
COPLEY, J. R. D. (1974). *Comput. Phys. Commun.* **7**, 289-317.
COPLEY, J. R. D. (1981). *Comput. Phys. Commun.* **21**, 431-436.
COPLEY, J. R. D., VERKERK, P., VAN WELL, A. A. & FREDRIKZE, H. (1986). *Comput. Phys. Commun.* **40**, 337-342.
FREDRIKZE, H. (1987). *Phys. Rev. A*, **36**, 2272-2287.
JOHNSON, M. W. (1974). *UKAEA.* Report AERE-R7682. United Kingdom Atomic Energy Authority.
MEARDON, B. H. (1973). *UKAEA.* Report AERE-R7302. United Kingdom Atomic Energy Authority.
PAALMAN, H. H. & PINGS, C. J. (1962). *J. Appl. Phys.* **33**, 2635-2639.
PRESS, W. H., FLANNERY, B. P., TENKOLSKY, S. A. & VETTERLING, W. T. (1986). *Numerical Recipes.* Cambridge Univ. Press.
SEARS, V. F. (1975). *Adv. Phys.* **24**, 1-45.

Contrast Formation in Synchrotron White-Beam Topographs

BY C. A. M. CARVALHO AND Y. EPELBOIN

Laboratoire de Minéralogie-Cristallographie, Universités P. M. Curie (Paris 6) et Paris 7, UA09 CNRS, 4 place Jussieu, 75252 Paris CEDEX 05, France

Abstract

It is shown theoretically that the contrast of synchrotron white-beam topographs, in most cases, is the superposition of the intensities produced by incoherent point sources situated on the entrance surface of the crystal. This is the reason for the similarity between synchrotron topographs and laboratory translation topographs. It is a consequence of the spectral width of the radiation and of the particle beam size and divergence in the storage ring. Upper and lower bounds are given for the coherence length. The natural collimation of synchrotron radiation and the effect of the source-to-crystal and crystal-to-film distances are taken into account. The results are valid for a large class of synchrotron sources.

I. Introduction

Synchrotron white-beam topography is an attractive technique for the investigation of crystal defects. Some of its advantages over laboratory topographs are imaging of large areas without moving the crystal, and shorter exposure times due to the high intensity of the beam. Many reflections can be recorded simultaneously, and the whole crystal always gives rise to an image, even when it is curved or highly distorted, due to the wide wavelength spectrum.

But synchrotron radiation is rather different from laboratory characteristic line radiation. Also, the distance between source and crystal differs by about two orders of magnitude from laboratory arrangements. This raises the question of the interpretation of the

0108-7673/90/060449-11$03.00

contrast of white-beam topographs, and of its relationship with laboratory topographic images. One important difference from laboratory experiments is harmonics superposition, because of the wide spectrum of the incident beam (Tuomi, Naukharinen & Rabe, 1974; Hart, 1975). However, Tanner, Midgley & Safa (1977) have shown that the contrast of dislocations is the same as in translation laboratory topographs when the amount of harmonics is negligible. Furthermore, Herres & Lang (1983) have shown that the contrast of many kinds of defects in synchrotron topographs with relevant harmonics contribution can be well reproduced by a superposition of laboratory images, taken at the harmonics wavelengths. It is thus experimentally established that, for each harmonic, the contrast of synchrotron white-beam topographs is the same as that of laboratory translation experiments, in spite of the differences in the diffraction conditions mentioned above.

Up to now there has been no theoretical explanation of this similarity. This is our objective in this paper. In § II we analyse the diffraction conditions for a monochromatic point source in the laboratory and synchrotron mountings, pointing out their differences. In § III we present a general analysis of the diffracted intensity, taking into account the wavelength spread and source size, which explains the similarity of the images. In § IV we consider the influence of the crystal-to-film distance.

This study is a preliminary to the writing of simulation programs for white-beam topographs, which will be published later.

II. Diffraction conditions for a point monochromatic source

Below, in order to simplify the notation we will represent constants that are not relevant to the problem as A_1, A_2, A_3 etc.

II.1. The incident wave

The electrical field $\mathbf{D}$ of the wave radiated by an electron is given by (Jackson, 1962)

$$\mathbf{D}(\mathbf{R}, \omega) = A_1 \omega [\exp(-i2\pi KR)/R]\mathbf{\Omega}(\mathbf{R}, \omega), \quad (1)$$

with

$$\mathbf{\Omega}(\mathbf{R}, \omega) = \int_{-\infty}^{\infty} \mathbf{n} \times (\mathbf{n} \times \boldsymbol{\beta})$$

$$\times \exp\{-i\omega[t - \mathbf{n}.\mathbf{r}(t)/c]\} \, dt. \quad (2)$$

$\mathbf{R}$ is the position vector of the observation point, $R = |\mathbf{R}|$, $\omega = 2\pi cK$, c is the speed of light, $K = 1/\lambda$, λ being the wavelength of the radiation, and $\mathbf{n}$ is a unit vector in the direction of $\mathbf{R}$. $\mathbf{r}$ is the position vector of the electron, t is the time and $\boldsymbol{\beta}$ the electron's velocity divided by c. Equations (1) and (2) are valid when $R \gg |\mathbf{r}|$. We see that, for each polarization, the

field is a spherical wave multiplied by a function of the direction of observation that describes the collimation of synchrotron radiation (2). The angular width in which this function varies appreciably is $1/\gamma$, where $\gamma = E/mc^2$, m is the electron's mass and E its energy in the storage ring (Jackson, 1962). For the machines used to produce X-rays, $1/\gamma$ must be of the order of 10^{-4} rad. Since the angular width of the X-ray rocking curve, $\Delta\theta$, is about 10^{-5} rad, $\Delta\theta$ is much smaller than $1/\gamma$. Thus, the vector $\mathbf{\Omega}$ in (2) is almost constant in the range $\Delta\theta$, and the incident wave may effectively be considered as a spherical wave.

This conclusion is in agreement with the fact that the contrast in experiments may be explained assuming that a spherical wave is incident on the crystal, just as in the laboratory. However, because of the large source-to-crystal distance in synchrotron mountings, the effective divergence of the incident wave is of the order of $\Delta\theta$, as we will explain in the next section.

II.2. The effective divergence of the incident wave

It is well known that the amplitude of the X-ray field at a point P_0 on the exit surface of the crystal is determined by the amplitude of the incident wave along the base BA of the Borrmann fan on the entrance surface (Fig. 1). Consequently, the effective divergence of the incident wave is α. We expect that, if $\alpha \gg \Delta\theta$, the incident wave may be considered as a spherical one. On the other hand, if $\alpha \ll \Delta\theta$, we expect that the intensity at the point P_0 will be the same as if the crystal were illuminated by a plane wave. Let us calculate the ratio $\Delta\theta/\alpha$.

For simplicity we consider the symmetrical case only. We may write

$$\alpha \simeq \tan\alpha = BA\cos\theta/L = 2t\sin\theta/L,$$

where θ is the Bragg angle, t is the crystal thickness and L is the source-to-crystal distance (Fig. 1). The width of the rocking curve of the perfect crystal in the symmetrical case is, neglecting the anomalous dispersion,

$$\Delta\theta = 2|\chi_h|/\sin 2\theta,$$
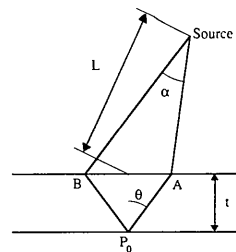
Fig. 1. Geometry of the wave incident on the crystal. α is the effective divergence, t is the crystal thickness and L is the source-to-crystal distance.

where χ_h is the hth Fourier component of the crystal polarizability. Thus,

$$\Delta\theta/\alpha = t_c/t, \quad \text{where} \quad t_c = |\chi_h|L/\sin\theta\sin2\theta. \quad (3)$$

In laboratory arrangements $L \sim 50$ cm. Taking $|\chi_h| \sim 10^{-6}$, $\theta = 10°$ and $t = 1$ mm, we get $\Delta\theta/\alpha \sim 10^{-2}$, so the incident wave may be considered as a spherical one. But in synchrotron arrangements L is much larger: taking $L = 30$ m as a typical value, we obtain $\Delta\theta/\alpha \sim 0.5$. Thus the effective divergence is only twice the width of the rocking curve, and the incident wave may no longer be considered as a spherical one.

In this section we used an argument in direct space to show that in synchrotron topographic arrangements the diffracted intensity distribution is not the same as that produced by a very divergent wave ($\alpha \gg \Delta\theta$), and that this is due to the large source-to-crystal distance. But in § II.1 we showed that the incident wave is, indeed, a spherical one, so that we may apply Kato's theory and get the usual intensity distribution along the exit surface of the crystal. This is a reasoning in reciprocal space, and it is in apparent contradiction with the one in direct space. This contradiction occurs because in Kato's theory, the source-to-crystal distance is not taken into consideration. This is because only part of the variation of the phase of the spherical wave on the entrance surface of the crystal is taken into account. Kato's approximation is valid for small source-to-crystal distances, but it is not valid for the distances usually employed for synchrotron topographs. A spherical-wave theory that takes into account second-order terms in the phase change along the entrance surface has been developed by Aristov, Polovinkina, Afanas'ev & Kohn (1980). These authors conclude that if $t_c \ll t$ [(3)] the diffraction is well described by Kato's treatment, and that if t_c is of the order of t a completely different fringe pattern appears. If $t_c \gg t$ the incident wave may be considered as a plane one. Their work confirms our qualitative direct-space argument, and brings the reciprocal-space argument into agreement with it. However, the analysis of Aristov *et al.* is rather heavy and the argument presented here gives a simple physical explanation of the situation.

Our considerations have shown that for a monochromatic spherical wave, that is, for radiation coming from a point source, synchrotron topographs should be quite different from laboratory translation images, because of the large source-to-crystal distance. But this is in contradiction with the experiments. In order to understand why this effect is not observed, we must take into account the radiation non-monochromaticity and the source size. This is explained in the next section in the general case of a deformed crystal.

III. The diffracted intensity on the exit surface of the crystal

To understand the mechanism of formation of the contrast, it is sufficient to consider the diffracted intensity for a single harmonic and one polarization state (parallel or perpendicular to the diffraction plane), since the final contrast will be the sum of these contributions. We first express the diffracted intensity at a point P_0 on the exit surface of the crystal as a function of the crystal characteristics, of the incident wave and of the wavelength λ by means of Takagi's theory. Then we analyse the influence of the wavelength bandwidth and of the source characteristics on the diffraction contrast.

III.1. Expression of the diffracted intensity as a function of the incident wavefield

Following Takagi (1969), we write the diffracted amplitude D_h at a point P on the exit surface of the crystal in the form

$$D_h = A_2(KC\chi_h\gamma_0/\sin 2\theta)$$
$$\times \exp\left[-i2\pi(\mathbf{k}+\mathbf{h}).\mathbf{R}\right]$$
$$\times \int_{BA} \nu_h(\xi)\varphi_0(\xi)\,d\xi. \quad (4)$$

Here $C = 1$ or $\cos 2\theta$ for parallel (σ) and perpendicular (π) polarization respectively and $\gamma_0 = \cos\psi_0$, ψ_0 being the angle between the incident beam and the normal to the crystal surface (Fig. 2). $\varphi_0 = \Psi_i \exp(i2\pi\mathbf{k}.\mathbf{R})$, where Ψ_i is the amplitude of the incident wave, that is, the component of the field $\mathbf{D}$ (1) in the plane of incidence or perpendicular to it, for π or σ polarization. BA is the base of the
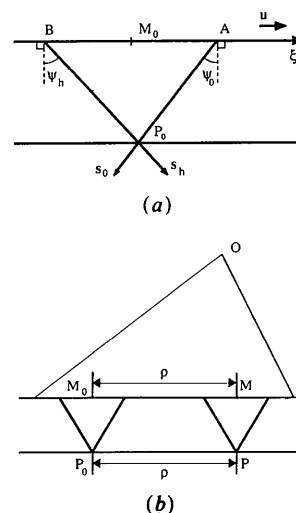
Fig. 2. (a) Geometrical parameters of the Borrmann fan. The vectors s_0 and s_h have the directions of the incident and diffracted beams respectively. u is a unit vector along the axis BA. (b) Relative positions of the points on the exit surface of the crystal. M_0 is the centre of the illuminated region.

Borrmann fan associated with point P_0 and ξ the coordinate along BA (Fig. 2a). ν_h is the Riemann function at the point P_0; it depends on the crystal parameters and on the deformation inside the Borrmann fan.

We also use a system of orthogonal axes with the x axis lying in the plane of the storage ring (assumed to be horizontal) and the y axis vertical, directed upwards. The z axis is oriented in the sense of circulation of the particles. For an insertion device the z axis is parallel to the axis of the device, with the plane $z = 0$ at the middle of its length. The origin is placed at the point where the trajectory of the synchronous particle traverses the plane $z = 0$ (Fig. 3a). For a bending magnet the z axis is tangent to the synchronous orbit at the origin. The position of the origin, on the orbit, is such that the point M_0 lies in the plane $x = 0$ (Fig. 3b). M_0 is the centre of the illuminated region of the entrance surface of the crystal.

We define the wavelength λ_0 so that the direction from the origin O (Fig. 3) to the point M_0 (Fig. 2b) makes a Bragg angle θ with the diffracting planes. Let $\mathbf{R}_0 = OM_0$ and $\mathbf{K}_0$ be a vector parallel to $\mathbf{R}_0$. We define $|\mathbf{K}_0| = K_0 = 1/\lambda_0$ ($\mathbf{K}_0$ then satisfies the Bragg law). For a general wavelength λ, $\mathbf{K}$ is the vector (in the plane of $\mathbf{R}_0$ and $\mathbf{h}$) of modulus $K = 1/\lambda$ that satisfies the Bragg law for the wavelength λ. The fact that the amplitude D_h varies with position inside the crystal permits us to choose the vector $\mathbf{k}$ (4) (Takagi, 1969). To simplify the equations we choose $\mathbf{k} = \mathbf{K}$.

Takagi (1969) writes the incident wave Ψ_i as a modulated plane wave. Here it is more convenient to write it in the form of a modulated spherical wave

$$\Psi_i = (\Psi_0/R) \exp(-i2\pi KR). \qquad (5)$$

Henceforth we will approximate the R in the denominator of (5) (but not in the argument of the

exponential) by R_0. It is then just a constant, and will be included in the constants A_n. We then obtain from (4)

$$D_h(K, P) = A_2(KC\chi_h\gamma_0/\sin 2\theta)$$
$$\times \exp[-i2\pi(\mathbf{K}+\mathbf{h}).\mathbf{R}]$$
$$\times \int_{-l/2}^{l/2} \nu_h(\xi)\,\Psi_0(\xi)$$
$$\times \exp[-i2\pi(KR - \mathbf{K}.\mathbf{R})]\,d\xi,$$

where l is the length of the segment BA (Fig. 2a).

Let us define $\mathbf{R} = \mathbf{R}_0 + (\rho + \xi)\mathbf{u}$, $\mathbf{u}$ being a unit vector directed along the ξ axis (Fig. 2a), ρ the distance along the exit surface of the crystal between the points P_0 and P (Fig. 2b), and $-l/2 \le \xi \le l/2$. Since $|\rho + \xi| \ll R_0$ we may assume that

$$R = \{[\mathbf{R}_0 + (\rho + \xi)\mathbf{u}]^2\}^{1/2}$$
$$\simeq R_0 + (\rho + \xi)\sin\psi_0 + \gamma_0^2(\rho + \xi)^2/2R_0.$$

Now, let $\Delta K_0 = K - K_0$. Keeping terms up to first order in $\Delta K_0/K_0$ we find that

$$KR - \mathbf{K}.\mathbf{R} \simeq KR_0 - \mathbf{K}.\mathbf{R}_0$$
$$- \gamma_0 \tan\theta\,\Delta K_0\rho + (K\gamma_0^2/2R_0)\rho^2$$
$$- K_0\gamma_0(\tan\theta\,\Delta K_0/K_0 - \gamma_0\rho/R_0)\xi$$
$$+ (K_0\gamma_0^2/2R_0)\xi^2.$$

The diffracted amplitude at P for wavenumber K is then

$$D_h(K, P) = A_3(KC\chi_h\gamma_0/\sin 2\theta)$$
$$\times \exp\left(-i2\pi K\left\{R_h + \left[\sin\psi_h\right.\right.\right.$$
$$\left.\left.- \gamma_h \tan\theta\frac{\Delta K_0}{K_0}\left(1+\frac{\gamma_0}{\gamma_h}\right)\right]\rho + \frac{\gamma_h^2\rho^2}{2R_h}\right\}\right)$$
$$\times \int_{-l/2}^{l/2} \nu_h(\xi)\,\Psi_0(\xi)\exp(-i2\pi K_0\gamma_0^2\xi^2/2R_0)$$
$$\times \exp\left[i2\pi K_0\gamma_0\left(\tan\theta\frac{\Delta K_0}{K_0} - \frac{\gamma_0\rho}{R_0}\right)\xi\right]d\xi,$$
$$(6)$$

where $\gamma_h = \cos\psi_h$ (Fig. 2a) and $R_h = R_0\gamma_h^2/\gamma_0^2$.

We remark that the coefficient of ξ in the argument of the exponential inside the integral depends both on $\Delta K_0/K_0$ and ρ. If ν_h and Ψ_0 do not depend on ρ, the diffracted intensity at point P, for wavenumber K, will be the same as the intensity at P_0 at the wavenumber K', so that $\tan\theta(K'-K_0)/K_0 = \tan\theta\,\Delta K_0/K_0 - \gamma_0\rho/R_0$. This means that the wavelength around which the diffraction takes place varies with the position on the exit surface of the crystal. It may be seen from Fig. 2(b) that $\lambda' = 1/K'$ is just the wavelength for which the direction OM

(a)

(b)

Fig. 3. The reference system: (a) Insertion device source. e is the particle. (b) Bending magnet source. M_0 is the point in the centre of the base of the Borrmann triangle associated with point P_0 (Fig. 2b).

makes a Bragg angle with the diffracting planes. To simplify the notation we write $(K' - K_0)/K_0 = \Delta K/K_0$. The significance of the phase factor in front of the integral wil be discussed in § IV.

Equation (6) gives the diffracted amplitude at P for one wavelength. The observed intensity I is the sum of $|D_h(K, P)|^2$ over the spectrum of wavelengths. So

$$I(P) = A_4 \frac{C^2|\chi_h|^2\gamma_0^2}{\sin^2 2\theta} \int\limits_{-l/2}^{l/2} d\xi \, d\xi' \nu_h(\xi) \nu_h^*(\xi')$$

$$\times \exp[-i2\pi K_0\gamma_0^2(\xi^2 - \xi'^2)/2R_0]$$

$$\times \int\limits_{-\Delta K_m/2}^{\Delta K_m/2} K^2\Psi_0(\xi)\Psi_0^*(\xi')$$

$$\times \exp[i2\pi\gamma_0 \tan\theta \Delta K(\xi - \xi')] \, d\Delta K, \quad (7)$$

where ΔK_m is the wavenumber bandwidth over which we sum. In the above expression we neglect the dependence of θ, χ_h and ν_h on the wavelength, since the range of ΔK is small.

Having expressed the diffracted intensity as a function of the incident field, we will now analyse the influence of the wavelength bandwidth and source characteristics on the diffracted intensity.

III.2. The coherence length of the incident wavefield

III.2.1. Wavelength band. We notice that the integration in ΔK in (7) is the Fourier transform of $K^2\Psi_0(K, \xi)\Psi_0^*(K, \xi')$ multiplied by a rectangular function of width ΔK_m. This is the integral representation of the mutual coherence function of the points ξ and ξ' (Born & Wolf, 1959, p. 500). We will first discuss its behaviour for sources that produce a very wide spectrum, such as bending magnets and wigglers, then for undulators that radiate a narrow spectrum.

For the case of a wide spectrum, we may consider that $K^2\Psi_0(K, \xi)\Psi_0^*(K, \xi')$ is practically constant in a small band where $\Delta\lambda_m/\lambda_0 = \Delta K_m/K_0 \ll 1$, so that the last integral in (7) will be proportional to $\sin[\pi\Delta K_m\gamma_0 \tan\theta(\xi - \xi')]/\pi\Delta K_m\gamma_0 \tan\theta(\xi - \xi')$. Thus, the relevant region of integration in ξ' along the entrance surface is such that

$$\Delta\xi = |\xi - \xi'| = [\gamma_0(\tan\theta)\Delta K_m]^{-1}$$

$$= \lambda_0[\gamma_0(\tan\theta)\Delta K_m/K_0]^{-1}. \quad (8)$$

We observe that $\Delta\xi$ is proportional to $\lambda_0/(\Delta\lambda/\lambda_0)$, the usual coherence length of the radiation (Born & Wolf, 1959, p. 500). Since the spectrum is very large, we may arbitrarily choose the value of ΔK_m. If we consider $\Delta K_m/K_0 = 10^{-3}$, which is the width of a characteristic line, $\lambda_0 = 1$ Å, $y_0 \simeq 1$ and $\tan\theta = 0.2$ ($\theta \sim 10°$), we find that $\Delta\xi \sim 0.5$ μm. In such a small region the Riemann function ν_h is practically constant

for nearly all crystals and defects, so that we may assume that $\nu_h(\xi') = \nu_h(\xi)$. We may also write $\exp[i2\pi K_0\gamma_0^2(\xi^2 - \xi'^2)/2R_0] = 1$. Further, we may approximate $\Psi_0(\xi')$ as $\Psi_0(\xi)$, since the angle subtended by a segment of about 0.5 μm at 30 m from the source is much smaller than $1/\gamma$. These approximations become better for larger values of ΔK_m. Thus, we may approximate the coherence function by $\delta(\xi - \xi')$, and the integration in ξ' will result in a constant. Equation (7) then becomes

$$I(P) = A_5(K_0^2C^2|\chi_h|^2\gamma_0^2/\sin^2 2\theta)$$

$$\times \int\limits_{-l/2}^{l/2} |\nu_h(\xi)|^2|\Psi_0(\xi)|^2 \, d\xi. \quad (9)$$

Let us consider the intensity at P_0 produced by a point source of unit strength situated at a point ξ_a on the segment BA (Fig. 2a). In this case $\Psi_0 = \delta(\xi - \xi_a)$, and from (7) we see that the intensity is $|K_0C\chi_h\gamma_0/\sin 2\theta|^2|\nu_h(\xi_a)|^2$. Thus, (9) means that the total diffracted intensity at P is the sum of the intensities produced by point sources of strength $|\Psi_0(\xi)|^2$ distributed along the entrance surface. There is no phase relationship between the amplitudes created by these sources. This is the meaning of the small width (8) of the correlation function mentioned above.

For values of ξ near the edges of the Borrmann triangle, the integration in ξ' will not cover the whole width of the coherence function, so that the integration in ξ' is in fact a function of ξ. But the region where this function of ξ is not constant is of the order of the width of the coherence function, which is very small compared with the length l of the base of the Borrmann fan, so that we may neglect this effect. The same remark applies to the rapid oscillations of the Riemann function near the edges of the triangle.

Let us now see what happens if the radiation is produced by an undulator. The spectrum is concentrated around the harmonics of the fundamental value ω_f, with a distribution $\Psi_0(\xi)\Psi_0^*(\xi)$ proportional to

$$\left\{\frac{\sin[N\pi(\omega/\omega_f - n)]}{N\pi(\omega/\omega_f - n)}\right\}^2,$$

where N is the number of periods of the undulator and n the order of the harmonic considered (Kitamura, 1980). The last integral in (7), which defines the correlation length $\Delta\xi$, is the Fourier transform of this function (the variation of K^2 is negligible within its width). This transform is a triangular function which is zero for $\Delta\xi > nN\lambda_0/\gamma_0 \tan\theta$. To estimate an upper bound of $\Delta\xi$, we take a large number of periods, say $N = 250$; for $\lambda_0 = 1$ Å, $\Delta\xi$ is smaller than 0.4 μm for the third harmonic, which is still a small value. Thus, the conclusion is the same for both types of sources.

Up to now we have considered only one particle in the storage-ring beam. To obtain the total intensity

effectively diffracted, we must sum the intensity given in (9) for all the particles of the beam, since the emissions of different electrons are not correlated. The particles in the beam are characterized by their position, direction of speed and energy, so we must sum (9) over these variables. But these integrations act only upon Ψ_0 and so do not change the form of the equation. As a result, $|\Psi_0(\xi)|^2$ represents the total intensity distribution of the incident beam along the base of the Borrmann fan.

We have shown that the diffracted intensity, at each point on the exit surface of the crystal, is the sum of the intensities of point sources situated along the entrance surface of the crystal. Thus, the contrast of the images does not depend on the source-to-crystal distance. This mechanism of image formation is the same as in laboratory translation topographs, and this is the reason that both kinds of images look similar. We have shown that this is due to the large spectral width of the incident beam. In the next section we will show that the size of the source leads to the same effect.

III.2.2. Influence of beam size and divergence.

The particles in a storage ring follow slightly different trajectories around the synchronous orbit, so that the radiated X-ray field varies [(1)]. Let us see what is the influence, for a fixed wavelength, of this field variation on the diffracted intensity.

The dynamic state of a particle, when it traverses the magnetic field region once, is characterized by its energy and by its position and velocity at a given time. We choose the origin of time so that $t = 0$ for $z = 0$. Let us call x_0 and y_0 the x and y coordinates of a general particle at $z = 0$. We define $x'_0 = dx/ds$ and $y'_0 = dy/ds$ at $z = 0$, s being the coordinate along the synchronous orbit. Since x'_0, $y'_0 \ll 1$, they are the angles that the velocity vector of the particle makes with the vertical and horizontal planes respectively (at $z = 0$). Further, let ΔE be the difference between the particle's energy E and the storage ring's norminal energy E_0.

To analyse the variation of the radiated field with the trajectory followed by the particle it is convenient to write the trajectory in the form

$$\mathbf{r}(t) = \mathbf{r}_0 + \mathbf{g}(t, E, x_0, y_0, x'_0, y'_0), \qquad (10)$$

where $\mathbf{r}_0 = x_0\mathbf{i} + y_0\mathbf{j}$, $\mathbf{i}$ and $\mathbf{j}$ being unit vectors along the x and y axes respectively. In general the vector $\mathbf{g}$ depends on x_0, y_0, x'_0, y'_0, E and on the magnetic field of the source. From (1), (2), (5) and (10) we get

$$\Psi_0 = A_6\omega \exp(i2\pi\mathbf{n}.\mathbf{r}_0)\Pi(\xi, \omega, E, x_0, y_0, x'_0, y'_0)$$

$$\equiv A_6\omega \exp(i2\pi\mathbf{n}.\mathbf{r}_0) \int_{-\infty}^{\infty} [\mathbf{n}' \times (\mathbf{n}' \times \boldsymbol{\beta})]_{\sigma,\pi}$$

$$\times \exp\{-i\omega[t - \mathbf{n}'.\mathbf{g}(t, E, x_0, y_0, x'_0, y'_0)/c]\} \, dt, \qquad (11)$$

where $\mathbf{n}'$ is a unit vector pointing from the point $\mathbf{r}_0$ to the point of observation, and the symbol $[\ ]_{\sigma,\pi}$ means the projection of $\mathbf{n}' \times (\mathbf{n}' \times \boldsymbol{\beta})$ in the directions of the σ or π polarizations respectively. Keeping terms up to the second order in $(\rho + \xi)/R_0$, x_0/R_0, y_0/R_0 and dropping an irrelevant constant, we may write

$$\mathbf{n}.\mathbf{r}_0 = [\gamma_0(\rho + \xi)/R_0](x_0 \cos \varphi + y_0 \sin \varphi), \qquad (12)$$

where θ_h and φ are the usual spherical coordinates of the vector $\mathbf{h}$, that is, $h_x = \sin \theta_h \cos \varphi$, $h_y = \sin \theta_h \sin \varphi$. Substituting (11) and (12) into (6) we find that the intensity produced by one particle is

$$I_K(P) = A_7 K^4 \gamma_0^2 |\chi_h|^2$$

$$\times \int_{-1/2}^{1/2} \nu_h(\xi)\nu_h^*(\xi')B\Pi(\xi)\Pi^*(\xi')$$

$$\times \exp[i2\pi\gamma_0 \tan \theta \, \Delta K(\xi - \xi')]$$

$$\times \exp\{i2\pi K_0\gamma_0[(\xi - \xi')/R_0]$$

$$\times (x_0 \cos \varphi + y_0 \sin \varphi)\} \, d\xi \, d\xi', \qquad (13)$$

with $B = \exp[-i2\pi K_0\gamma_0^2(\xi^2 - \xi'^2)/2R_0]$. We have omitted the other variables in the argument of Π for clarity.

To obtain the total intensity we must multiply $I_K(P)$ by the average number of electrons in each dynamic state and sum over the states. The average number of particles in a state of energy difference ΔE is (Elleaume, 1986)

$$f_E(\Delta E) = A_8 \exp[-\tfrac{1}{2}(\Delta E/\sigma_E)^2], \qquad (14)$$

where σ_E is a parameter of the storage ring that describes the energy dispersion of the electron beam.

To analyse the spatial and angular dispersions we consider, for the moment, a reference system with the z axis directed along the tangent to the synchronous orbit at $z = 0$. We represent the quantities in this system by capital letters, e.g. Y_0, Y'_0. The spatial and angular dispersions in the vertical plane are due to the betatron oscillations (for a plane ring). The average number of particles with a displacement Y_0 and an angle Y'_0 is (Elleaume, 1986)

$$f_y(Y_0, Y'_0) = A_9 \exp[-\tfrac{1}{2}(Y_0^2/\sigma_y^2)]$$

$$\times \exp[-\tfrac{1}{2}(Y'_0 - Q_y Y_0)^2/\sigma_{y'}^2], \qquad (15)$$

with

$$\sigma_y^2 = \varepsilon_y \beta_y, \quad \sigma_{y'}^2 = \varepsilon_y/\beta_y, \quad Q_y = \beta'_y/2\beta_y.$$

Here ε_y is the ring's vertical emittance, β_y is the vertical betatron function at $z = 0$, $\beta'_y = d\beta_y/ds$. In the orbit plane, X_0 and X'_0 are the sum of a betatron contribution X_b and an off-energy contribution: $X_0 = X_b + \eta\Delta E/E_0$, $X'_0 = X'_b + \eta'\Delta E/E_0$. η is the dispersion function of the ring at $z = 0$ and $\eta' = d\eta/ds$. For a given ΔE the betatron position is then $X_b = X_0 - \eta\Delta E/E_0$ and the average number of particles in

each state is

$$f_x(X_0, X_0') = A_{10} \exp\left[-\tfrac{1}{2}(X_0 - \eta\Delta E/E_0)^2/\sigma_x^2\right]$$
$$\times \exp\{-\tfrac{1}{2}[X_0' - \eta'\Delta E/E_0$$
$$- Q_x(X_0 - \eta\Delta E/E_0)]^2/\sigma_{x'}^2\}, \qquad (16)$$

where σ_x and Q_x have the same meanings as σ_y and Q_y. We must now express X_0, Y_0, X_0', Y_0' in terms of x_0, y_0, x_0', y_0'. For a bending magnet the tangent of the synchronous orbit is directed along the z axis, so that $X_0 = x_0$ etc. For insertion devices the tangent of this orbit makes a small angle with the device axis, which is the z axis, so that we may assume that $X_0 = x_0$ and $Y_0 = y_0$ with a negligible error. Also, for the small rotations involved, the angles are additive, so that $Y_0' = y_0' - y_{0s}'$, y_{0s}' being the value of y_0' for the synchronous particle, and similarly for the state x_0, x_0'. Consequently, the number of particles in the state y_0, y_0' is $f_y(y_0, Y_0')$.

The number of particles in a state x_0, y_0, x_0', y_0', ΔE is proportional to the product of (14), (15) and (16), because the distributions are not correlated. Using (13) we get for the total intensity at point P, with wavenumber K,

$$I_K(P) = A_{11}K^4|\chi_h|^2\gamma_0^2 \int_{-l/2}^{l/2} d\xi\, d\xi'\, \nu_h(\xi)\nu_h^*(\xi') B$$

$$\times \exp\left[i2\pi\gamma_0 \tan\theta\, \Delta K(\xi - \xi')\right]$$

$$\times \int_{-\infty}^{\infty} \Pi(\xi)\Pi^*(\xi') \exp\{i2\pi K_0\gamma_0[(\xi - \xi')/R_0]$$

$$\times (x_0\cos\varphi + y_0\sin\varphi)\}$$

$$\times \exp(-\tfrac{1}{2}y_0^2/\sigma_y^2) \exp\left[-\tfrac{1}{2}(Y_0' - Q_y y_0)^2/\sigma_{y'}^2\right]$$

$$\times \exp\left[-\tfrac{1}{2}(x_0 - \eta\Delta E/E_0)^2/\sigma_x^2\right]$$

$$\times \exp\{-\tfrac{1}{2}[X_0' - \eta'\Delta E/E_0$$

$$- Q_x(x_0 - \eta\Delta E/E_0)]^2/\sigma_{x'}^2\}$$

$$\times d\Delta E\, dx_0\, dy_0\, dX_0'\, dY_0'. \qquad (17)$$

We notice that the integrations over the dynamic variables of the electron beam define a function of ξ and $\Delta\xi$ that is a kind of correlation length. In general this function depends not only on the size of the electron beam, as usual in optics, but also on its divergence and energy spread. However, we will see that in most cases this function may be considerably simplified.

It is possible to show that $\Pi(\xi, \omega, E_0 + \Delta E, x_0, y_0, x_0', y_0') \simeq \Pi(\xi, \omega + \Delta\omega, E_0, x_0, y_0, x_0', y_0')$, with $\Delta\omega/\omega \simeq 2\Delta E/E_0$. Thus, a change in the energy of the particle is roughly equivalent to a change in wavelength. For most storage rings $\Delta E/E_0 \simeq 10^{-3}$. This means that the variation of Π with the energy of the particle will be important only if the wavelength band emitted by the source is of the order of 10^{-3} (such as in the case of an undulator with a very large number of periods). But this happens only rarely, so

that we will neglect the variation of Π with the energy in (17). Performing the integration in ΔE we obtain

$$I_K(P) = A_{12}K^4|\chi_h|^2\gamma_0^2 \int_{-l/2}^{l/2} d\xi\, d\xi'\, \nu_h(\xi)\nu_h^*(\xi') B$$

$$\times \exp\left[i2\pi\gamma_0 \tan\theta\, \Delta K(\xi - \xi')\right]$$

$$\times \int_{-\infty}^{\infty} \Pi(\xi)\Pi^*(\xi')$$

$$\times \exp\{i2\pi K_0\gamma_0[(\xi - \xi')/R_0]$$

$$\times (x_0\cos\varphi + y_0\sin\varphi)\}$$

$$\times \exp(-\tfrac{1}{2}y_0^2/\sigma_y^2)$$

$$\times \exp\left[-\tfrac{1}{2}(Y_0' - Q_y Y_0)^2/\sigma_{y'}^2\right]$$

$$\times \exp(-\tfrac{1}{2}x_0^2/\sigma_x^2)$$

$$\times \exp\left[-\tfrac{1}{2}(X_0' - Q_x x_0)^2/\sigma_{x'}^2\right]$$

$$\times dx_0\, dy_0\, dX_0'\, dY_0'. \qquad (18)$$

Here,

$$\sigma_x^2 = \beta_x\varepsilon_x + \eta^2(\sigma_E/E_0)^2,$$

$$Q_x = [(\beta_x'/2)\varepsilon_x + \eta'\eta(\sigma_E/E_0)^2]/\sigma_x^2,$$

$$\sigma_{x'}^2 = \varepsilon_x\left\{\varepsilon_x + \left(\frac{\sigma_E}{E_0}\right)^2\left[\left(1 + \frac{\beta_x'}{4}\right)\frac{\eta^2}{\beta_x}\right.\right.$$

$$\left.\left. - \beta_x'\eta'\eta + \beta_x\eta'^2\right]\right\}\bigg/\sigma_x^2.$$

We notice that the convolution in energy results in a function of the same form as (16), but with the parameters σ_x, $\sigma_{x'}$ and Q_x changed. This means that the energy spread of the particles results in an increase of the horizontal size and divergence of the beam, when the radiated field Π does not depend on ΔE.

The integrations in x_0' and y_0' result in a function of ξ, x_0 and y_0 that describes the total intensity, observed at the point ξ, produced by the particles that traverse the plane $z = 0$ at the point x_0, y_0 (Fig. 3). When multiplied by the Gaussian function of x_0, y_0, it represents the intensity distribution of the source seen from point ξ on the entrance surface of the crystal. Thus the integration in x_0, y_0 is the Fourier transform of the source intensity distribution, that is, the source-correlation length (Born & Wolf, 1959, p. 508). The only difference is that this correlation length depends on the observation point, because of the collimation of synchrotron radiation.

In general the function Π depends on x_0 and y_0 through the vectors $\mathbf{n'}$ and $\mathbf{g}$ (11). Let us write the x component of the vector $\mathbf{g}$ (10) in the form $g_x = cx_0't + p_x(t, E_0, x_0, y_0, x_0', y_0')$, and similarly for the y component. If the functions p_x and p_y are independent of x_0, y_0, x_0' and y_0', then the function $\Pi(\xi, \omega, E_0, x_0, x_0', y_0, y_0')$ may be shown to be of the form $\Pi(\omega, E_0, n_x - x_0/R_0 - x_0', n_y - y_0/R_0 - y_0')$, where n_x and n_y are the x and y components of the

vector $\mathbf{n}$. In this case the integration in x_0' and y_0' is simply a convolution. This is true for a bending magnet, but not for an insertion device, because the magnetic field depends on x and y (Brown, Halbach, Harris & Winick, 1983). So the functions p depend on x_0, y_0 (and also on x_0' and y_0'). However, this dependence is usually small, in the range of values where the distributions of (15) and (16) are relevant, because the beam will always be near the axis of the device. Thus we may neglect it in most cases. The correlation function Corr then takes the simpler form

$$\text{Corr} = A_{13}G(\xi - \xi') \int_{-\infty}^{\infty} |\Pi(n_x - q_x, n_y - q_y)|^2$$

$$\times \exp\left[-\tfrac{1}{2}q_x^2/(\sigma_{Rx}^2 + \sigma_{x'}^2)\right]$$

$$\times \exp\left[-\tfrac{1}{2}q_y^2/(\sigma_{Ry}^2 + \sigma_{y'}^2)\right]$$

$$\times \exp\left\{ i2\pi K_0\gamma_0[(\xi - \xi')/R_0] \right.$$

$$\times \left[\frac{(1/R_0 + Q_x)\sigma_x^2 \cos\varphi}{\sigma_{Rx}^2 + \sigma_{x'}^2} q_x \right.$$

$$\left. \left. + \frac{(1/R_0 + Q_y)\sigma_y^2 \sin\varphi}{\sigma_{Ry}^2 + \sigma_{y'}^2} q_y \right] \right\} dq_x\, dq_y \qquad (19)$$

where

$$\sigma_{Rx;y}^2 = \sigma_{x;y}^2 (Q_{x;y} + 1/R_0)^2,$$

$$G(\xi - \xi') = \exp\left\{ -\frac{1}{2}\left[2\pi K_0\gamma_0 \frac{(\xi - \xi')}{R_0} \right]^2 \right.$$

$$\left. \times \left(\frac{\sigma_x^2\sigma_{x'}^2 \cos^2\varphi}{\sigma_{Rx}^2 + \sigma_{x'}^2} + \frac{\sigma_y^2\sigma_{y'}^2 \sin^2\varphi}{\sigma_{Ry}^2 + \sigma_{y'}^2} \right) \right\}.$$

The correlation function is now the product of two terms. The first is the Gaussian function G, which depends only on the electron beam characteristics and the source-to-crystal distance. The second term, the integral, depends both on the radiated field and on the electron beam, and describes the influence of the collimation of synchrotron radiation on the coherence length. Let us consider for the moment only the terms that vary in the vertical plane. It may be shown that when $|\Pi|^2$ is much wider than $\sigma_{y'}(1 + \sigma_R^2/\sigma_{y'}^2)^{1/2}$, the correlation length is

$$\Delta\xi_s = (\lambda_0/2\pi\gamma_0)(R_0/\sigma_y).$$

In this case the correlation length depends only on the source size, and the intrinsic collimation of the radiation has no influence on it. As far as the coherence length is concerned, we may consider that the source emits a spherical wave. This is usually the case for low-emittance storage rings.

When $|\Pi|^2$ is much narrower than $\sigma_{y'}(1 + \sigma_R^2/\sigma_{y'}^2)^{1/2}$ the correlation length is determined by the Gaussian G. This is usualy the case for high-emittance storage

rings. The coherence length becomes

$$\Delta\xi_m = \Delta\xi_s(1 + \sigma_R^2/\sigma_{y'}^2)^{1/2}.$$

This is equivalent to having a smaller effective source size σ_e, such that

$$\Delta\xi_m = (\lambda_0/2\pi\gamma_0)(R_0/\sigma_e), \qquad (20a)$$

with

$$\sigma_e = \sigma_y(1 + \sigma_R^2/\sigma_{y'}^2)^{-1/2}$$

$$= \sigma_y\left[1 + \left(\frac{\beta_y}{R_0} + \frac{\beta_y'}{2} \right)^2 \right]^{-1/2}. \qquad (20b)$$

The reduction of the effective source size is due to the collimation of synchrotron radiation.

$\Delta\xi_m$ and $\Delta\xi_s$ are the upper and lower bounds respectively for the correlation length, regardless of the form of the emitted radiation. We observe that when $\sigma_R \ll \sigma_{y'}$, $\Delta\xi_m = \Delta\xi_s$, so that the correlation length is independent of the form of the radiated field [this may also be seen from (19)]. All these arguments apply when we consider the plane of the orbit [except the last form of (20b)].

From (19) and (20) we get the following expression for $\Delta\xi_m$:

$$\Delta\xi_m/R_0 = (\lambda_0/2\pi\gamma_0)(\sigma_{ex}^2 \cos^2\varphi + \sigma_{ey}^2 \sin^2\varphi)^{-1/2} \qquad (21)$$

The maximum value of this expression depends on the angle φ if $\sigma_{ex}^2 \neq \sigma_{ey}^2$, which is usually the case. Since the beam size is usually smaller in the vertical direction, the maximum occurs for $\varphi = \pi/2$ [see (11)], that is, when the diffraction vector is in the vertical plane. For a small value for σ_{ey}, say 0·05 mm, we get from (21) that $\Delta\xi/R_0 \simeq 3 \times 10^{-7}$ for $\lambda = 1$ Å. This is about two orders of magnitude smaller than the natural divergence of synchrotron radiation, $1/\gamma$, so we have assumed $\Pi(\xi') = \Pi(\xi)$ in (18).

For a low-emittance storage ring, a typical value of σ_{ex} is 0·5 mm. Thus, for $\lambda_0 = 1$ Å and $R_0 = 30$ m, we get from (21) $\Delta\xi \simeq 1$ μm for $\varphi = 0$, so that we may still assume $\nu_h(\xi) = \nu_h(\xi')$ and $B = 1$ [see (12)] in most cases. This means that the total observed intensity is the superposition of the intensities produced by point sources on the entrance surface of the crystal, as for the wavelength spread (9). For reflections with the $\mathbf{h}$ vector perpendicular to the plane of the orbit $\varphi = 90°$, and $\Delta\xi$ is of the order of 5 μm for $\sigma_{ey} = 0·1$ mm. In these cases we may no longer assume $\nu_h(\xi) = \nu_h(\xi')$, so that the reduction of the expression of the diffracted intensity to a sum of the intensities of incoherent point sources is due only to the radiation polychromaticity. For a high-emittance storage ring, σ_y is usually greater than 0·5 mm, so that the radiation is incoherent for all diffraction directions.

IV. Effect of the crystal-to-film distance

To calculate the intensity on the exit surface of the crystal we have added the intensities produced by all the points of the source, for all the wavelengths. However it is well known that, beyond the crystal, the diffracted beams produced by different point sources and at different wavelengths propagate in different directions. Consequently, the intensity on the film is the superposition of the intensities of different points of the exit surface of the crystal. This intensity, on the crystal surface, is the sum of the intensities produced by the fraction of source points and wavelengths for which the diffracted beams propagate along the same direction. This fact must be taken into account in the analysis of the mechanism of image formation in the film, since the major factor of this mechanism is the coherence length, which is in turn determined by the source size and wavelength band. Thus, we will first determine the intensity at a point on the exit surface of the crystal, for all source points and wavelengths whose diffracted beams propagate along the same direction after the crystal. We call this intensity partial intensity.

The diffracted beam propagates in the incidence plane, that is, the plane parallel to the diffraction vector $\mathbf{h}$ that contains the point P on the exit surface of the crystal and the source point. As the source extends across the incidence plane, the partial intensity is now the sum of the intensities produced only by the points of the source belonging to the line of intersection of the source surface and the incidence plane. Let us consider one of these source points. In the incidence plane, the direction of propagation of the diffracted beam varies with the wavelength by an amount $\tan \theta \, \Delta\lambda_0/\lambda_0$, because of the change in the Bragg angle. In the case of synchrotron topographs there is an additional change, due to the variation of phase of the incident spherical wave along the entrance surface of the crystal. In fact, the phase factor before the integral in (6) shows that the diffracted field is a modulated spherical wave coming from a virtual source situated at a distance $R_h = R_0\gamma_h^2/\gamma_0^2$ from the entrance surface, along a line that makes an angle $\psi_h + \tan \theta \, \Delta\lambda_0/\lambda_0(1+\gamma_0/\gamma_h)$ with this surface (Fig. 4). Thus, for any given point on the exit surface of the crystal, the change in the direction of propaga-

tion of the radiation due to a change in wavelength, $\delta\psi_h$, is (for a crystal with parallel faces)
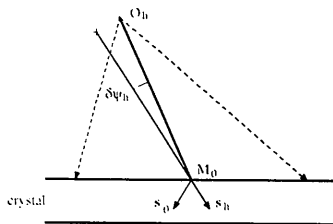
$$\delta\psi_h = (\Delta\lambda_0/\lambda_0) \tan \theta(1 + \gamma_0/\gamma_h). \quad (22)$$

We notice that this change in the direction of propagation of the diffracted beam is always greater than the usual value $\tan \theta \, \Delta\lambda_0/\lambda_0$. For a symmetrical reflection $\delta\psi_h$ is twice as large, and more than this if the incident beam is normal to the crystal surface. The origin of the extra term may be interpreted geometrically as follows. Let us assume that the crystal is perfect and that the effective divergence of the incident wave is negligible ($\alpha \ll \Delta\theta$, § II.2). For simplicity we consider the symmetric case only. In this case the intensity profile along the exit surface of the crystal, for the wavelength λ_0, is a rocking curve, with the angular deviation from the Bragg angle, $\delta\theta$, being given by $\gamma_0\rho/R_0$ (Fig. 5). This may be seen from (6): in this case the quadratic term in ξ may be neglected, and the integral becomes the Fourier transform of the Riemann function. This is the amplitude diffracted when a plane wave is incident on the crystal, and the square of its modulus is the rocking curve. The diffracted beam is a wavepacket, centred at the point P_0, and it propagates beyond the crystal along the average direction $\mathbf{K}_0 + \mathbf{h}$. Each point on the entrance surface receives a wave with a different value of $\delta\theta$. Since, in the symmetric case, each ray is mirror reflected in the lattice planes, each point, on the exit surface, radiates a ray that makes an angle $\delta\theta$ with the direction $\mathbf{K}_0 + \mathbf{h}$. Thus, the diffracted beam is a divergent wave. For the wavelength λ the beam is a wavepacket centred at point P (so that $\gamma_0\rho/R_0 = \tan \theta \, \Delta\lambda_0/\lambda_0$) and it propagates along the average direction $\mathbf{K} + \mathbf{h}$. The angle between these two average directions is the usual value $\tan \theta \, \Delta\lambda_0/\lambda_0$. To obtain $\delta\psi_h$, at a given point, say P_0, we must add the angle between $\mathbf{K}_0$ and $\mathbf{K}$ to the angle $\delta\theta$ between the rays coming out from P_0 and P. The result is (22).

To calculate the partial intensity we use a system of coordinates x_1 and y_1, which may be expressed in terms of x_0 and y_0 by a rotation of an angle φ about the z axis. When we take into account the different

Fig. 4. Position, for wavelength λ, of the virtual source O_h of the spherical diffracted wave.
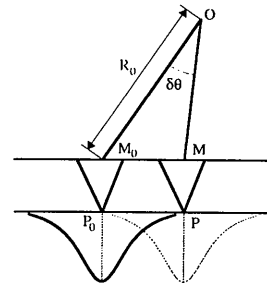
Fig. 5. Geometrical interpretation of the change in the direction of propagation of the diffracted beam. The continuous line is the intensity profile for the wavelength λ_0 and the dashed line is the profile for wavelength λ.

point sources in the diffraction plane there is an extra term that contributes to the change in the direction of propagation, that comes from (12). The total change in direction of propagation, $\Delta\psi_h$, is

$$\Delta\psi_h = \frac{\Delta\lambda_0}{\lambda_0}\tan\theta + \frac{\gamma_0}{\gamma_h}\left(\frac{\Delta\lambda}{\lambda_0}\tan\theta + \frac{x_1}{R_0}\right).$$

The second term of this equation, which does not exist in laboratory topographs, is due to the fact that the whole crystal is illuminated by a spherical wave. This is itself a consequence of the large source-to-crystal distance.

The partial intensity is given by (18), where, instead of integrating over x_0, y_0 and ΔK, we now integrate over the new coordinate x_1 and ΔK, under the restriction that $\Delta\psi_h$ be constant. This means that the integrations in x_1 and ΔK are not independent. As a result, using the arguments of the preceding section, we obtain the coherence length after the crystal, $\Delta\xi_v$:

$$\Delta\xi_v = \Delta\xi_m(1 + \gamma_0/\gamma_h)$$
$$\times\left[1 + \frac{\sin^2 2\varphi}{4}\frac{(\sigma_{ex}^2 - \sigma_{ey}^2)^2}{\sigma_{ex}^2\sigma_{ey}^2}\right]^{1/2}. \quad (23)$$

We observe that $\Delta\xi_v$ is greater than $\Delta\xi_m$ by a factor $(1 + \gamma_0/\gamma_h)$. Furthermore, there is an increase in $\Delta\xi_v$ if the dimensions of the electron beam in the vertical and horizontal planes are different. This effect may be noticeable if the beam is very flat. When $\sigma_{ex} = 5\sigma_{ey}$ the coherence length increases by a factor of 2·6 for $\varphi = 45°$.

To obtain $\Delta\xi_v$ we have reasoned as if the diffracted beam propagated by means of rays, as in geometrical optics. This intuitive argument may be justified rigorously on the basis of the Huygens–Fresnel principle, and it is valid if the film is near the crystal (less than about 10 cm, if the contrast is nearly constant in a region of 2 μm along the crystal surface).

When the correlation length $\Delta\xi_v$ is small enough, the intensity at a point on the crystal surface is still the sum of the intensities of incoherent point sources, as we have seen before. In this case the diffracted wavelength band is determined by the effective source size [this may be seen from (18)], and the intensity distribution on the film is simply a convolution of the intensity on the crystal surface with a Gaussian function. Thus, except for a loss of resolution, the contrast on the film is the sum of the contrasts produced by incoherent point sources on the entrance surface of the crystal.

We have seen, in the preceding section, that for low-emittance storage rings the coherence length $\Delta\xi_m \simeq \Delta\xi_s < \Delta\xi_v$ is not small enough. In the plane of diffraction, the intensity reaching a point in the film will be the sum of the intensities of the points situated in a region whose size is the product of $\Delta\psi_h$ by the crystal-to-film distance, d. The value of $\Delta\psi_h$ is determined by the wavelength band diffracted by the crys-

tal and the effective source size. Two cases must be considered. When the variation of the contrast in the region $d\Delta\Psi_h$ is negligible, we may neglect the variation of the Riemann function with the point P. As we are summing the intensities for different $\Delta\psi_h$, we may integrate separately over x_1 and ΔK in (18), which means that (9) remains valid. This happens when d is small enough, and corresponds to the situation where there is no resolution loss in the plane of diffraction. The contrast in the film is thus the same as on the crystal surface, except for a possible loss of resolution in the direction perpendicular to the diffraction plane. A typical value of d is 5 cm. If we assume $\theta = 10°$, $\gamma_0/\gamma_h \simeq 1$ and $\Delta\lambda/\lambda_0 = 3\times10^{-4}$, we get (neglecting the term x_1/R_0 for low-emittance rings) $d\Delta\psi_h = 6$ μm. In this range, the contrast may not be considered as constant for the most distorted regions of a crystal. In this case the contrast in the film may not be described as a superposition of the contrasts produced by incoherent point sources on the crystal entrance surface. The experimental parameters, such as the source-to-crystal distance, influence the observed contrast and synchrotron topographs will no longer resemble laboratory ones. This might be the case at the ESRF station, and new contrast would be observed.

We have considered explicitly the case of a crystal with plane surfaces. Clearly this is a good approximation when the bending radius of the surfaces is much greater than the source-to-crystal distance. This restriction is not important in laboratory mountings, where $R_0 \simeq 40$ cm, but it is much more drastic in synchrotron arrangements, where $R_0 \simeq 30$ m. However, it may be shown without difficulty that our results remain valid if the crystal surfaces are curved, provided that the local radius of curvature is not much smaller (about 1/10) than R_0, which is seldom the case. Furthermore, the results of § III are also valid for the Bragg case (for thick crystals), since the integral representation of the diffracted amplitude, (4), is also applicable in this case (Uragami, 1969). The propagation of the beam after the crystal is more complicated than in the Laue case.

V. Concluding remarks

We have shown that the contrast on the exit surface of the crystal is the superposition of the intensities produced by incoherent point sources situated on its entrance surface, in spite of the large distance between the source and the crystal. This is the reason for the similarity between synchrotron and laboratory topographs, and it is due to the small coherence length of synchrotron radiation. The coherence length is determined by the wavelength bandwidth and the electron-beam characteristics in the storage ring. We have determined the upper and lower bounds of the source coherence length. The lower bound does not

depend on the collimation of synchrotron radiation; it is determined by the source size, as in usual optics. The upper bound is inversely proportional to the effective source size, and it is independent of the magnetic field of the source point in the storage ring. The upper bound is larger than the lower one because of the collimation of synchrotron radiation. When both the electron beam divergence and the ratio source size/source-to-crystal distance are small, compared with the intrinsic divergence of the radiation, the source coherence length is near its lower bound. This is usually the case in low-emittance storage rings. When the above ratio is large compared with the radiation divergence, as happens for high-emittance rings, the coherence length is near its upper bound. However, the coherence length is usually shorter in the latter case than in the former one.

The contrast on the film is the same as on the exit surface of the crystal, except for a resolution loss, when the source correlation length is much smaller than the distance where the contrast along the crystal surface varies appreciably. This is the situation for high-emittance storage rings. For low-emittance rings this is not true if the contrast varies rapidly (*e.g.* dislocation images), unless the film is very near the crystal. However, such contrast modifications, which take place only in small regions of the image (where the contrast varies rapidly enough), are difficult to

observe, because of the resolution loss. Thus, in the analysis of practical experiments, we may consider that the contrast of synchrotron white-beam topographs is the superposition of the images produced by incoherent point sources situated on the entrance surface of the crystal.

References

ARISTOV, V. V., POLOVINKINA, V. I., AFANS'EV, A. M. & KOHN, V. G. (1980). *Acta Cryst.* A36, 1002–1013.
BORN, M. & WOLF, E. (1959). *Principles of Optics.* London, New York, Paris, Los Angeles: Pergamon.
BROWN, G., HALBACH, K., HARRIS, J. & WINICK, H. (1983). *Nucl. Instrum. Methods,* 208, 65–77.
ELLEAUME, P. (1986). *Cours de l'École d'Été de Rayonnement Synchrotron, Aussois, France.* Paris: Editions CNRS.
HART, M. (1975). *J. Appl. Cryst.* 8, 436–444.
HERRES, N. & LANG, A. R. (1983). *J. Appl. Cryst.* 16, 47–56.
JACKSON, W. D. (1962). *Classical Electrodynamics,* p. 479. New York: Wiley.
KITAMURA, H. (1980). *Jpn. J. Appl. Phys.* 19, L185–L188.
TAKAGI, S. (1969). *J. Phys. Soc. Jpn,* 26, 1239–1253.
TANNER, B. K., MIDGLEY, D. & SAFA, M. (1977). *J. Appl. Cryst.* 10, 281–286.
TUOMI, T., NAUKHARINEN, K. & RABE, P. (1974). *Phys. Status Solidi A,* 25, 93–106.
URAGAMI, T. (1969). *J. Phys. Soc. Jpn,* 27, 147–154.

Image Deconvolution of a Single High-Resolution Electron Micrograph*

By LIU YI-WEI, XIANG SHI-BIN, FAN HAI-FU,† TANG DONG AND LI FANG-HUA‡

Institute of Physics, Chinese Academy of Sciences, Beijing, China

PAN QING

Centre of Structure Analysis, University of Science and Technology of China, Hefei, China

AND N. UYEDA AND Y. FUJIYOSHI

Institute of Chemical Research, Kyoto University, Kyoto, Japan

Abstract

An X-ray crystallographic method has been introduced into the image processing of high-resolution electron microscopy. This enables the deconvolution of single electron micrographs of a crystalline sample. For this purpose the chemical composition of the sample should be known approximately, the image should be taken near the optimum defocus condition, but no preliminary knowledge of the crystal structure is needed. The method has been proved to be efficient with a high-resolution electron micrograph of chlorinated copper phthalocyanine taken on the Kyoto 500 kV electron microscope.

---

* Part of this paper was presented at the IUCr Summer School on Crystallography and Its Teaching, Tianjin, China (1988).
† To whom correspondence should be addressed.
‡ Also at CCAST (World Laboratory), PO Box 8730, Beijing, China.